nuclear fusion
IAEA

Overview of TJ-II experiments

To cite this article: C. Hidalgo *et al* 2005 *Nucl. Fusion* **45** S266

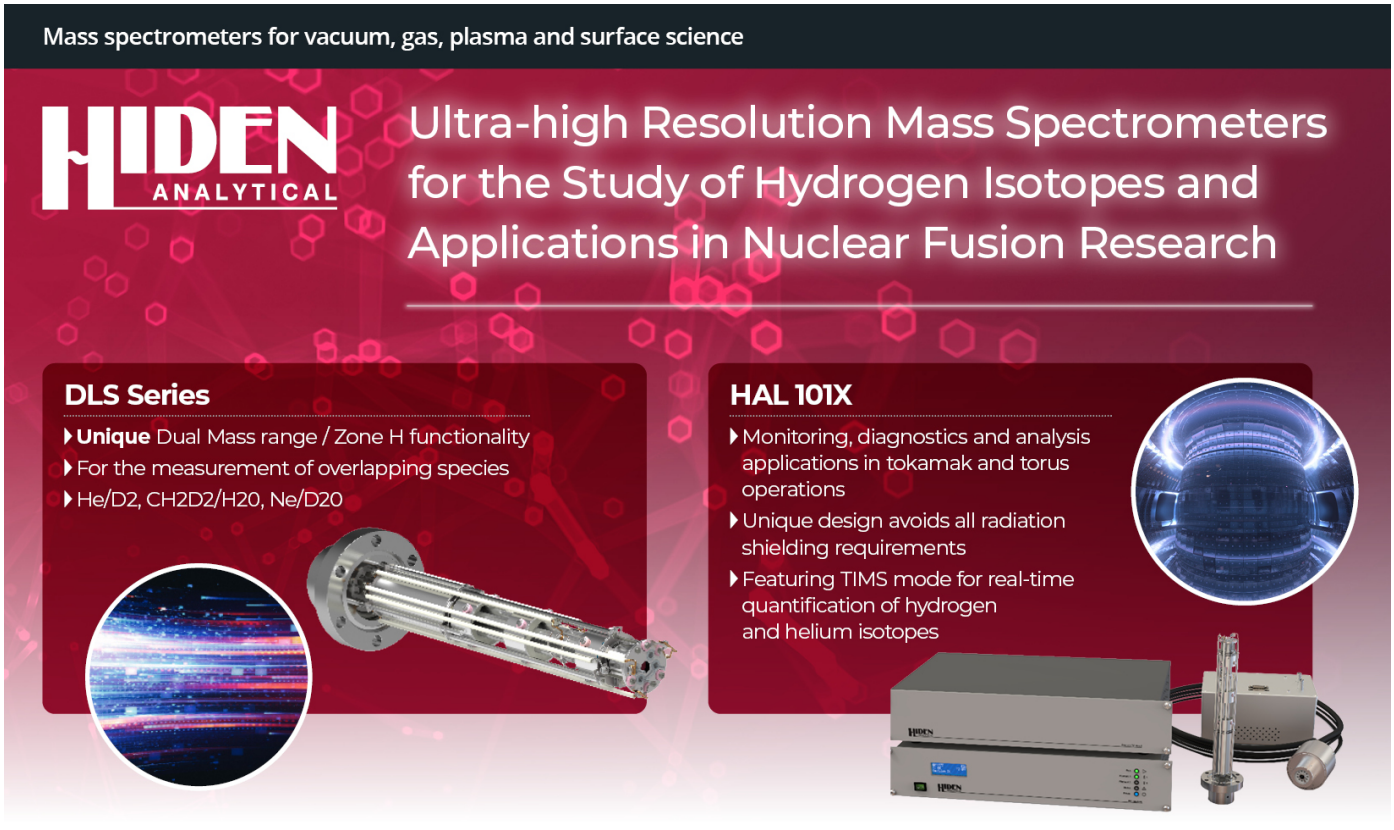

INSTITUTE OF PHYSICS PUBLISHING and INTERNATIONAL ATOMIC ENERGY AGENCY NUCLEAR FUSION

Nucl. Fusion **45** (2005) S266–S275 doi:10.1088/0029-5515/45/10/S22

Overview of TJ-II experiments

C. Hidalgo[1], C. Alejaldre[1], A. Alonso[1], J. Alonso[1], L. Almoguera[1], F. de Aragón[1], E. Ascasíbar[1], A. Baciero[1], R. Balbín[1], E. Blanco[1], J. Botija[1], B. Brañas[1], E. Calderón[1], A. Cappa[1], J.A. Carmona[1], R. Carrasco[1], F. Castejón[1], J.R. Cepero[1], A.A. Chmyga[1], J. Doncel[1], N.B. Dreval[2], S. Eguilior[1], L. Eliseev[3], T. Estrada[1], J.A. Ferreira[1], A. Fernández[1], J.M. Fontdecaba[4], C. Fuentes[1], A. García[1], I. García-Cortés[1], B. Gonçalves[5], J. Guasp[1], J. Herranz[1], A. Hidalgo[1], R. Jiménez[1], J.A. Jiménez[1], D. Jiménez-Rey[1], I. Kirpitchev[1], S.M. Khrebtov[2], A.D. Komarov[2], A.S. Kozachok[2], L. Krupnik[2], F. Lapayese[1], M. Liniers[1], D. López-Bruna[1], A. López-Fraguas[1], J. López-Rázola[1], A. López-Sánchez[1], E. de la Luna[1], G. Marcon[1], R. Martín[1], K.J. McCarthy[1], F. Medina[1], M. Medrano[1], A.V. Melnikov[2], P. Méndez[1], B. van Milligen[1], I.S. Nedzelskiy[5], M. Ochando[1], O. Orozco[1], J.L. de Pablos[1], L. Pacios[1], I. Pastor[1], M.A. Pedrosa[1], A. de la Peña[1], A. Pereira[1], A. Petrov[6], S. Petrov[7], A. Portas[1], D. Rapisarda[1], L. Rodríguez-Rodrigo[1], E. Rodríguez-Solano[1], J. Romero[1], A. Salas[1], E. Sánchez[1], J. Sánchez[1], M. Sánchez[1], K. Sarksian[6], C. Silva[5], S. Schchepetov[6], N. Skvortsova[6], F. Tabarés[1], D. Tafalla[1], A. Tolkachev[1],V. Tribaldos[1], I. Vargas[1], J. Vega[1], G. Wolfers[1] and B. Zurro[1]

[1] Laboratorio Nacional de Fusión, EURATOM-CIEMAT, 28040 Madrid, Spain
[2] Institute of Plasma Physics, NSC KIPT, 310108 Kharkov, Ukraine
[3] Institute of Nuclear Fusion, RNC Kurchatov Institute, 123182 Moscow, Russia
[4] Universitat Politècnica de Catalunya, 08034 Barcelona, Spain
[5] Associação EURATOM/IST, Centro de Fusão Nuclear, 1049-001 Lisboa, Portugal
[6] General Physics Institute, Russian Academy of Sciences, 119991 Moscow, Russia
[7] A.F. Ioffe Physical Technical Institute, 194021 St Peterburg, Russia

E-mail: carlos.hidalgo@ciemat.es

Received 11 November 2004, accepted for publication 15 April 2005
Published 7 October 2005
Online at stacks.iop.org/NF/45/S266

Abstract

This paper presents an overview of experimental results and progress made in investigating the role of magnetic configuration on stability and transport in the TJ-II stellarator. Global confinement studies have revealed a positive dependence of energy confinement on the rotational transform and plasma density, together with different parametric dependences for metallic and boronized wall conditions. Spontaneous and biasing-induced improved confinement transitions, with some characteristics that resemble those of previously reported H-mode regimes in other stellarator devices, have been observed. Also, magnetic configuration scan experiments have shown an interplay between magnetic structure (rationals, magnetic shear), transport and electric fields. Although the dc radial electric fields are comparable with those expected from neoclassical calculations, additional mechanisms based on neoclassical/turbulent bifurcations and kinetic effects are needed to explain the impact of magnetic topology on flows and radial electric fields. Hydrocarbon fuelling experiments in configurations with a low-order rational value in the rotational transform located in the proximity of the last closed flux surface ($n = 4/m = 2$) have shown the impurity screening properties related to the expected divertor effect. The first TJ-II experiments in neutral beam injection plasmas are reported.

PACS numbers: 52.55.-s, 52.55.Hc, 52.25.Fi

(Some figures in this article are in colour only in the electronic version)

1. Introduction

The TJ-II heliac ($B(0) \leqslant 1.2\,\mathrm{T}$, $R(0) = 1.5\,\mathrm{m}$, $\langle a \rangle \leqslant 0.22\,\mathrm{m}$, $P_{\mathrm{ECH}} \leqslant 600\,\mathrm{kW}$, $P_{\mathrm{NBI}} \leqslant 2\,\mathrm{MW}$) offers unique characteristics that make it a very suitable tool to investigate the complex phenomenology that interrelates electric field, instabilities, magnetic configuration and transport in fusion plasmas. It possesses a large range of achievable magnetic configurations ($0.9 \leqslant \iota(0)/2\pi \leqslant 2.2$) and low magnetic shear that allows for accurate control of the low-order rationals present in the rotational transform profile. Its magnetic well is the main stabilizing mechanism [1]. The magnetic well depth (up to 6%) can be almost suppressed in the edge region [2].

The results presented in this paper have been obtained in plasmas created and heated with electron cyclotron resonance heating (ECRH) ($2 \times 300\,\mathrm{kW}$ gyrotrons, at 53.2 GHz, second harmonic, X-mode polarization) and neutral beam injection (NBI). The ECRH is coupled to the plasma through two quasi-optical transmission lines, placed at positions symmetric about the stellarator, and equipped with an internal steerable mirror. In this context, second harmonic breakdown simulations that take electron–electron collision processes into account have been performed [3] to compute the temporal evolution of different species and the breakdown time. The first experiments with NBI heated plasmas have been performed in the TJ-II stellarator [4]. Beams of 400 kW port-through (H_0) power at 28 kV, are injected on to target plasmas created using one or two ECRH lines. Ongoing developments include plasma heating by Bernstein waves (a new system is being designed for TJ-II). In particular, the O-X-B1 scheme can provide full power deposition for densities above $1.3 \times 10^{13}\,\mathrm{cm}^{-3}$.

This paper is organized as follows: in section 2, TJ-II global confinement and improved confinement regimes are reviewed. In section 3, recent transport studies are reported. Plasma wall studies are discussed in section 4. Properties of NBI plasmas are reported for the first time in section 5. Finally, conclusions are presented in section 6.

2. Global confinement, enhanced confinement modes and magnetic topology

The dependence of the TJ-II global energy confinement time on plasma parameters has been investigated in metal and boronized wall conditions [5]. The parametric dependence of confinement shown by the all-metal wall data set follows the ISS95 scaling [6] except for the rotational transform dependence, which appears to be higher in TJ-II (0.6 versus 0.4). After boronization the situation changes. The dependence on rotational transform becomes weaker (0.35 instead 0.6) although marginally congruent with ISS95, but the density dependence becomes much stronger (1.06 instead 0.51). Global confinement becomes better, as shown in figure 1, the pre-factor in the scaling law increases by a factor of 2.3, from $10^{-1.88} = 0.013$ to $10^{-1.53} = 0.030$, although with different parametric dependences. This increase in confinement must be taken as a qualitative reference only because the strong change in density dependence hinders the interpretation of the comparison.

The observed differences have been explained as being due to the modified plasma wall interaction after boronization,

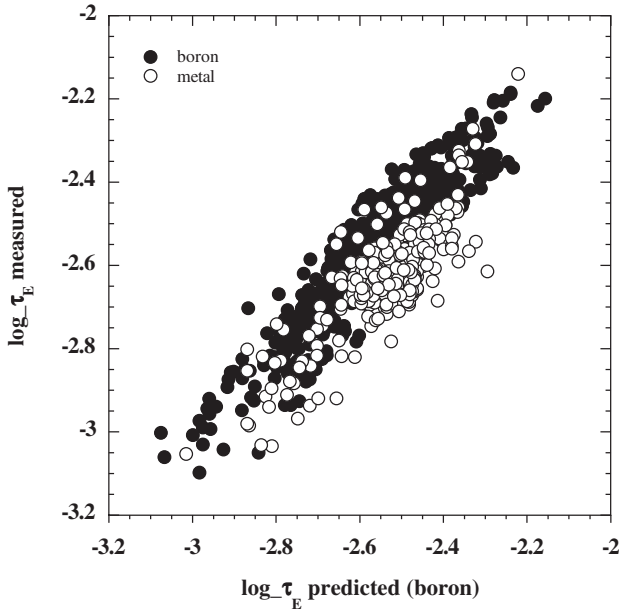

Figure 1. Experimental confinement time versus best fit for boronized wall data set (●). Metal wall data (○) are shown with the same fit for comparison.

as well as due to the different features of the enhanced particle confinement mode found in TJ-II [7], depending on the wall conditions. The measurement of the radiated power is not available for all the discharges included in the database; therefore, it has not been considered in the calculation of the global energy confinement time. However, it can be argued that it does not play the main role in accounting for the observed difference in confinement between all-metal and boron wall plasmas: the available measurements of radiated power in all-metal wall plasmas (16% of the shots in the database) yield relatively low values, with fractions in the range between 7–29% of the port-through power ($19 \pm 0.4\%$ being the mean value and 19% also the median value). The radiated power is substantially decreased after boronization, dropping typically by a factor of 3. Had we taken into account the radiated power, by assuming that it is 19% and 6% in the all-metal and boron cases, respectively, we would have obtained $10^{-1.74} = 0.018$ and $10^{-1.49} = 0.032$ for the corresponding pre-factors. Still, the confinement would be a factor 1.8 better for the boron plasmas than for the all-metal wall plasmas.

TJ-II results support the ISS95 conclusion regarding the beneficial influence of increasing the rotational transform on global energy confinement, at least for low magnetic shear devices. This support is relevant because the $\iota/2\pi$-range in TJ-II data is considerably wider than the ISS95 one.

2.1. Spontaneous transitions and development of $E \times B$ sheared flows

Spontaneous transitions to improved confinement regimes have already been observed in TJ-II. An enhanced particle confinement regime was found for plasmas created in an all-metal scenario [7,8]. It consists of a spontaneous transition to a highly peaked density profile mode that in turn leads to a decay in the electron density in the edge region and

to an increase in total particle content. This mode leads to an increase in the global particle confinement time by a factor greater than three. The conditions under which the transition to this mode was achieved for all-metal walls included a predefined trimming of the gas-puff waveform and a critical density, $\langle n_e \rangle_{crit} \sim 6 \times 10^{18}\,m^{-3}$. For boronized-wall conditions the transition was obtained under different recycling/gas puffing conditions. Another type of spontaneous improvement in particle and energy confinement has been observed in some TJ-II plasmas. Again, this is triggered by the only external knob [9], i.e. the fuelling rate.

Recent experiments have shown that the development of the naturally occurring edge velocity shear layer requires a minimum plasma density in the TJ-II stellarator [10, 11]. The increase in the edge shearing rate is correlated with the increase in turbulent velocity fluctuations. These results, consistent with transition models of turbulence driven flows, might provide the underlying physics of spontaneous TJ-II transitions.

As the plasma density increases, the edge ion saturation current and its radial gradient increases, and the floating potential becomes more negative in the plasma edge (figure 2). Because the edge temperature profile (in the range of 20–30 eV) is rather flat in the TJ-II plasma periphery, the radial variation in the floating potential signals directly reflects changes in the radial electric field (E_r), which turns out to be radially inwards in the plasma edge as the density increases above $0.5 \times 10^{19}\,m^{-3}$. The local turbulent particle flux also shows an increase near the critical density and tends to slightly decrease as sheared flow develops (figure 3). The magnitudes of the spontaneously developed shearing rates have been compared with those measured during biasing induced improved confinement regimes in TJ-II (see below), suggesting that spontaneous sheared flows and fluctuations are near marginal stability [10, 11]. Electron density and temperature profile evolution show a broadening in the density profile above the critical density while the temperature profile remains similar, reflecting the strong impact of plasma density in the TJ-II global confinement scaling.

2.2. *Effect of transformer induced toroidal current in confinement*

Stellarators are currentless devices in which the only toroidal current sources are bootstrap and RF induced currents. In TJ-II, these currents can be compensated to some extent by means of the internal movable mirrors on the two quasi-optical ECRH lines. Also, TJ-II has an Ohmic (OH) transformer capable of inducing toroidal plasma currents up to 10 kA. Previously, it was found that plasma confinement improves by inducing a negative (with respect to the magnetic field) OH current [12], i.e. making the rotational transform more negative thus increasing negative magnetic shear (figure 4). Conversely, a positive current was shown to degrade confinement [12]. The asymmetry found suggested searching magnitudes that may have changed sign under induction, e.g. the toroidal electric field and/or the global magnetic shear (as TJ-II vacuum rotational transform profiles are almost shearless). Hence, discrimination experiments to separate their roles were designed and performed [13].

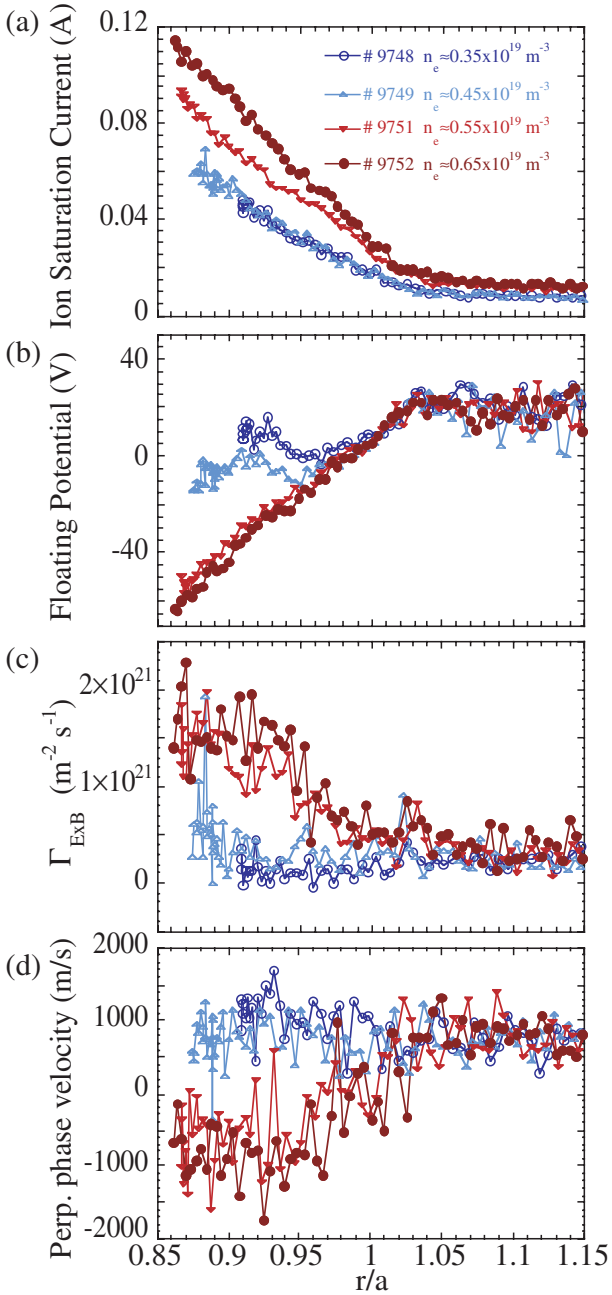

Figure 2. Radial profiles of (*a*) the ion saturation current, (*b*) the floating potential, (*c*) the local turbulent transport and (*d*) the deduced perpendicular velocity obtained for different values of the line-averaged density in a plasma configuration with $\iota(a)/2\pi \approx 1.7$.

These discrimination experiments consisted in comparing discharges with and without electron cyclotron current drive (ECCD) (i.e. changing the plasma current, I_p, while maintaining the toroidal electric field, E_t) that shared the same transformer action (which affects both I_p and E_t): i.e. if the plasma responds to E_t, then no delay between the start of Ohmic induction and plasma response should be found among discharges with different ECCD levels and conversely. Moreover, in order to make temporal discriminations with low ECCD levels the discharges to be compared must have similar

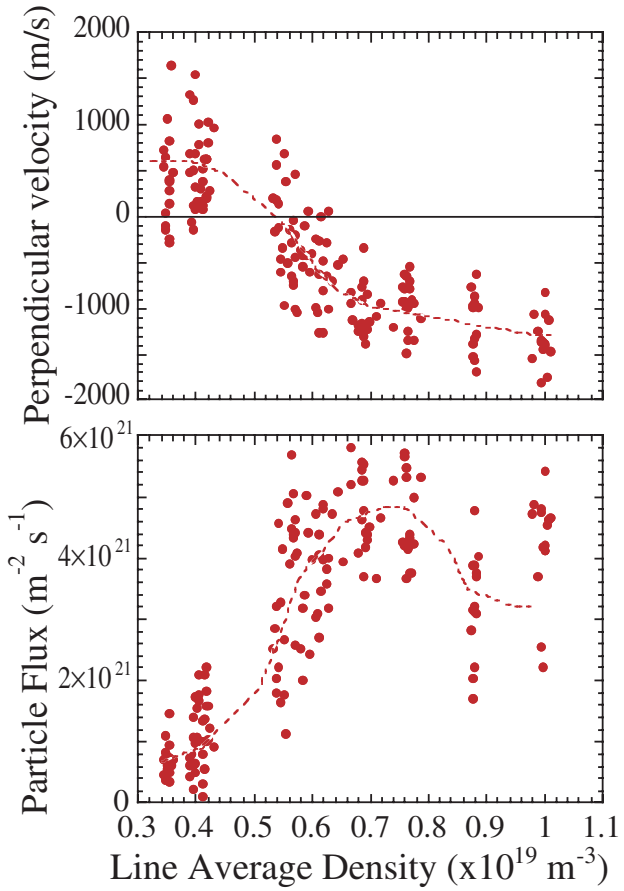

Figure 3. Perpendicular phase velocity and turbulent particle flux measured at $r/a \approx 0.8$ in plasmas with different line-averaged densities. Dotted lines are guides for the eye.

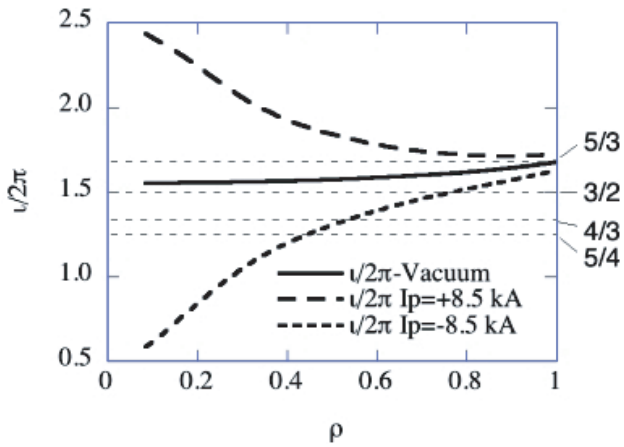

Figure 4. Influence of plasma current on rotational transform profiles. In the present experiment the induced OH current is negative (with respect to the magnetic field) and, therefore, it decreases the rotational transform.

density values and need reference discharges without current drive. The experiments showed that significant changes in plasma densities are related to the induced I_p, but not to E_t (figure 5). Studying the relation between density and I_p we found that, in the range of induced I_p, the average density $\langle n_e \rangle$ behaves as follows: for positive $I_p \leqslant 5$ kA $\langle \tilde{n}_e \rangle$ decreases; for

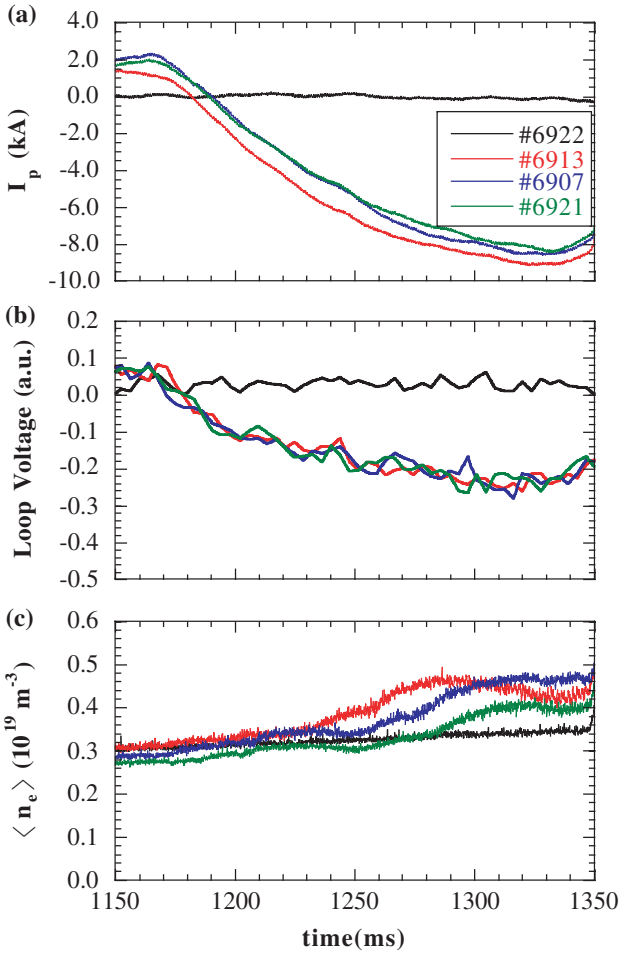

Figure 5. Time evolution of net plasma current (*a*), loop voltage (*b*) and line-averaged density (*c*) in a set of four discharges: a reference one without induction (in black) and three discharges with equal transformer action but different ECCD: negative (#6913), null (#6917) and positive (#6921).

negative $I_p \leqslant 5$ kA, $\langle n_e \rangle$ increases, and for $|I_p| \geqslant 5$ kA, $\langle n_e \rangle$ increases.

A clear advantage of Ohmic currents is that their profile can be reasonably inferred. Assuming that the actual knob for these observations is the global magnetic shear via plasma currents, then not only its magnitude, but also its sign, plays a role in confinement. Three complementary possibilities are suggested: (i) MHD stability: helical MHD modes can exist in TJ-II; their stability is dependent on the magnetic field, rotational transform and shear. (ii) Modification of particle orbits: this may affect considerably the fraction of direct particle losses in TJ-II. These losses can affect very differently the populations of passing and trapped particles, depending on the rotational transform of the configuration. (iii) Turbulent driven transport: instabilities such as trapped electron modes depend both on local and global magnetic shear.

2.3. Electron internal transport barriers and role of rationals

The generation of internal and edge transport barriers is linked to plasma regions with a unique magnetic topology. In configurations with low or negative magnetic shear, internal

transport barriers (ITBs) are formed close to the location of a minimum in the safety factor ($q_{\min}$) and in the proximity of low-order rational surfaces [14]. Edge transport barriers are located close to the boundary between the region with open and closed magnetic field lines.

Electron transport barriers have been observed in ECRH plasmas in stellarator devices and in plasma regimes with high heating power density [15–18]. These transitions are characterized by centrally peaked electron temperature profiles together with an improvement in core electron heat confinement.

Transport barriers close to resonant magnetic surfaces have been reported [19, 20]. This result has been interpreted on the basis of an increase of the sheared $E \times B$ flow linked to the radial location of rational surfaces [21, 22]. An alternative interpretation is based on the rarefaction of resonant surfaces in the proximity of low-order rationals, which is expected to decrease turbulent transport [23–25]. The relation of low-order rational surfaces and transport is a topic of ongoing discussion [26].

The influence of the magnetic topology on e-ITB formation has recently been experimentally studied in the TJ-II stellarator [27]. A configuration scan (where iota was changed from 1.55 to 1.61) has shown that the plasma current value at which this transition takes place depends on the magnetic configuration. In this experiment, the induced OH current is negative (with respect to the magnetic field) and therefore it decreases the rotational transform. Experimentally, we observe that the higher the rotational transform the higher the plasma current (in absolute value) needed for the transition. This result points to the presence of a low-order rational surface ($n = 3/m = 2$) close to the plasma core as being a necessary condition for triggering e-ITB formation [27]. Kinetic effects induced by ECRH also play an important role for e-ITB triggering in this low collision regime [28].

HIBP measurements have permitted characterization of the plasma potential profile during e-ITB formation. The plasma potential increases in the plasma core region. As a consequence, the radial electric field increases from about $5\,\mathrm{kV\,m^{-1}}$ before to $15\,\mathrm{kV\,m^{-1}}$ during the e-ITB (figure 6). Simultaneous measurements of the total beam intensity (proportional to plasma density) indicate that, at the transition, plasma density profiles are more hollow.

Transient behaviour with a rapid reduction in the core electron temperature, interpreted as the annihilation and creation of e-ITBs, was found in TJ-II plasmas with a rational surface close to the plasma core. The transient behaviour in the plasma potential takes place on a time scale of about 50 μs, which is much shorter than the energy confinement time, and it is dynamically coupled with perturbations in the core electron temperature and plasma density [27]. During these transients, some magnetic activity was detected by Mirnov coils. Often, this activity appears also in the ECE signals [29].

2.4. Biasing induced improved confinement regimes

Experimental results have shown that it is possible to modify global and edge plasma parameters with both positive and negative biasing (i.e. an inner limiter biased positive or negative with respect to an outer limiter). Figure 7 shows the

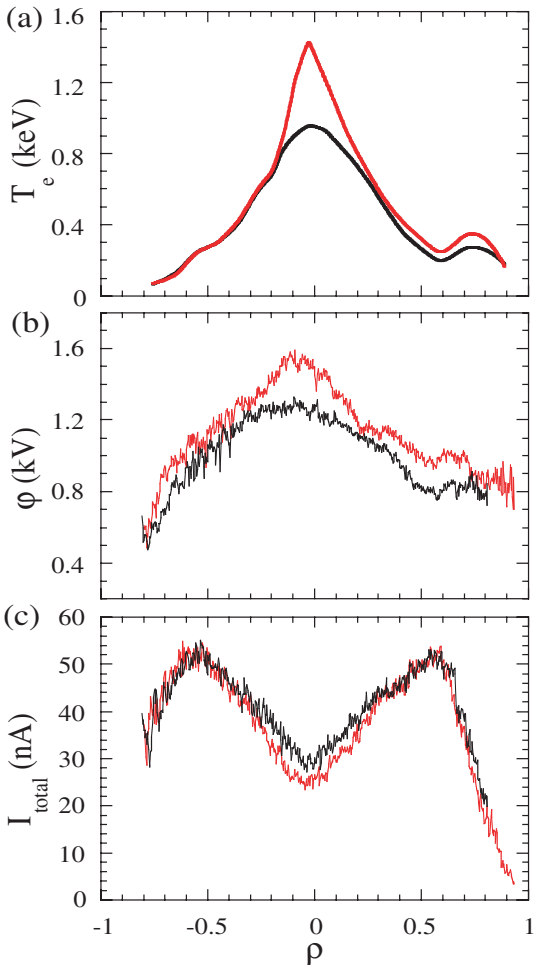

Figure 6. Plasma profiles before (black) and during (grey) the e-ITB: (*a*) electron temperature, (*b*) plasma potential and (*c*) beam intensity.

temporal evolution of plasma density, H_α monitors and edge $E \times B$ turbulent transport under negative biasing. The ratio between plasma density (n_e) and particle recycling, as quantified by H_α monitors, increases by up to a factor of 2 during negative limiter biasing together with a significant reduction in the turbulence level. Bursty-type behaviour in the H_α monitors, and evidence of MHD instabilities, has been observed during improved confinement regimes. Experimental results show the clear impact of these edge instabilities on (particle) confinement. The degree of modification of plasma confinement depends on different parameters: biasing voltage, plasma density as well as the radial location and the driven current of the biased limiters [30].

Edge as well as core plasma potentials are modified on two different time scales. In the rapid time scale (10–100 μs), the plasma potential changes in both the edge and core regions; in the slow time scale (1–10 ms) plasma potential modifications are linked to the evolution in the plasma density. The experimental results obtained can shed some light on quantifying the importance of neoclassical mechanisms when compared with anomalous ones in the study of the damping of the radial electric fields and flows in fusion plasmas.

Measurements of density and electron temperature profiles obtained by Thomson scattering during the negative

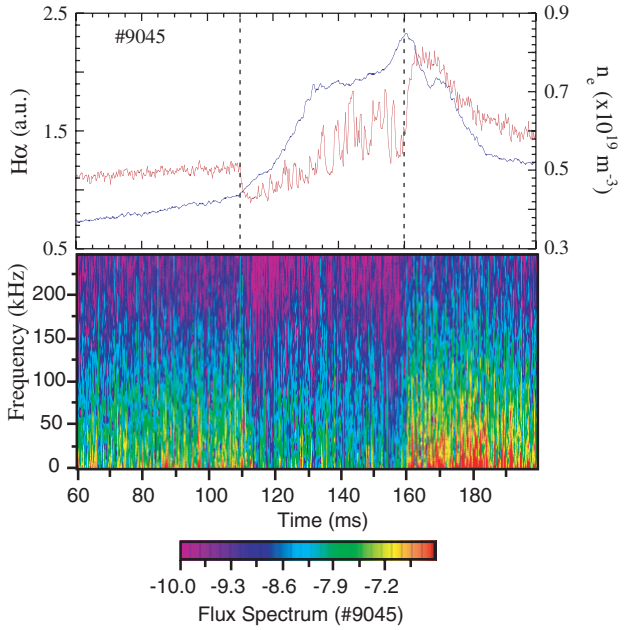

Figure 7. Line-averaged density and H_α signals and edge $E \times B$ turbulent transport during edge negative biasing.

biasing phase show that the density profile broadens while the temperature profile remains similar. An edge radial electric field, of the order of 100 V cm^{-1}, was measured by means of the HIBP diagnostic during the negative limiter biasing phase. Although radial electric fields are mainly modified in the proximity of the biased limiter, the plasma potential is affected across the whole plasma [31].

It was also determined that, during limiter biasing, the spectral line intensities from inherent plasma impurities increase in proportion with the line-averaged electron density. Furthermore, the bolometer arrays, used to monitor the total radiation emitted along discharges, helped to show that the increase in total radiation observed during limiter biasing could be uniquely attributed to the increase in electron density, i.e. the electron temperature remained constant. The results and analysis of the data collected provide, by their consistency, significant evidence that limiter biasing in the TJ-II does not induce significant influxes of impurities from the outer plasma region [32]. The phenomenology of TJ-II improved confinement regimes looks similar to the H-mode regimes previously reported in stellarators ([18, 33, 34] and references therein).

3. Transport studies

3.1. Impurity and particle transport studies

Transport studies on impurities injected into plasmas by the laser ablation method have been undertaken in various stellarators with the aim of obtaining localized information on transport coefficients in such devices. Previous experiments in TJ-II have shown that the decay of the perturbation created by the ablation can be analysed using a stretched exponential (of the type, $A_1 \exp[-((t - t_0)/\tau)^\beta]$) and the impurity confinement times reach up to 100 ms [35].

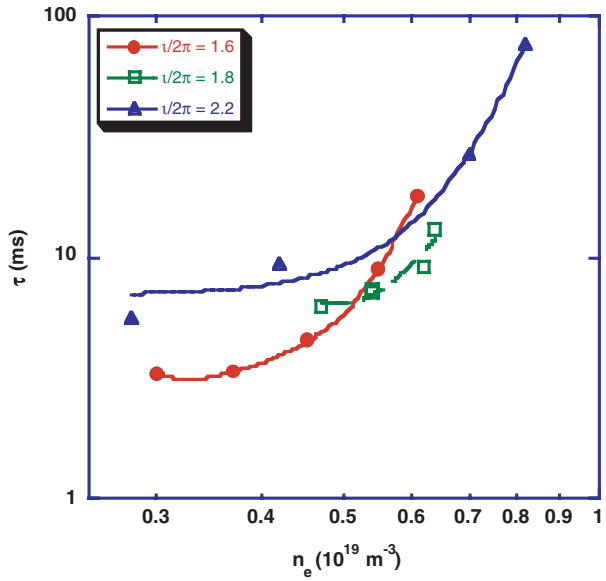

Figure 8. Impurity (Si) confinement time versus plasma density for three different magnetic configurations.

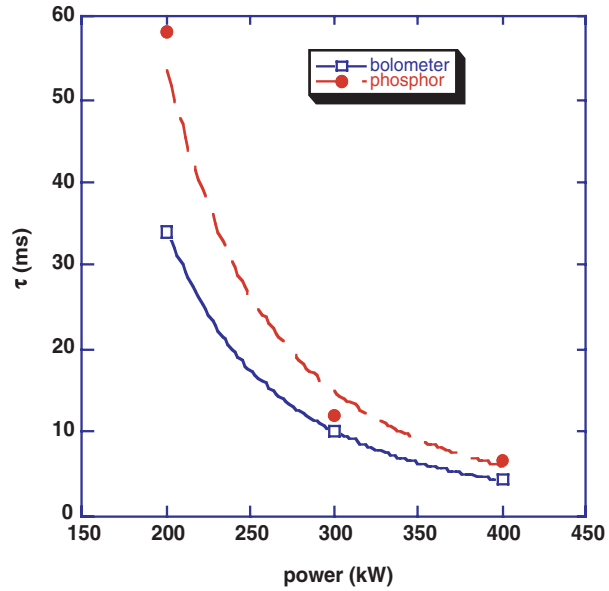

Figure 9. Influence of ECRH heating on impurity (Si) confinement time.

Recently, impurity transport has been investigated for a broad range of experimental situations in electron cyclotron heated plasmas (ECRH): i.e. for a density scan, a magnetic configuration scan, a power scan and its dependence on power deposition profile [36]. Figure 8 shows the dependence of impurity confinement for three different magnetic configurations ($\iota/2\pi = 1.6$, 1.8 and 2.2) and at several densities. The confinement time (τ) slowly increases with density up to a certain point, where it increases more rapidly. Furthermore, this turning density is found to be higher for higher rotational transform values. Such behaviour resembles the spontaneous improvement in plasma bulk particle confinement at a critical density. The influence of ECRH power on impurity confinement time is shown in figure 9. Confinement time shows a strong dependence on ECRH heating power ($\tau \approx P^{-3}$), which

turns out to be stronger than the one observed in the global energy confinement time ($P^{-0.6}$).

It is useful to compare impurity and particle diffusivities in TJ-II. It is found that the impurity diffusion coefficient increases towards the plasma centre, where most of the injected power is deposited and that diffusion increases with power, most notably at the plasma core. The convective velocity is typically directed inwards at radii less than $\rho \approx 0.5$ and outwards at larger radii. Similar behaviour was reported in the W7-AS device [37]. Impurity diffusivities of the order of $0.5\,\mathrm{m^2\,s^{-1}}$ ($\rho \approx 0.6$) and particle diffusivities in the range $0.2\,\mathrm{m^2\,s^{-1}}$ ($\rho \approx 0.6$) have been measured [35, 38].

However, evidence of non-diffusive transport mechanisms has been clearly observed during the propagation of edge cooling pulse experiments [39]. These studies have led to a reconsideration of diffusive transport, based on the continuous time random walk. A one-fluid toy model has been developed, incorporating a critical gradient mechanism that separates a sub-critical diffusive and a super-critical anomalous transport channel, depending on the local value of the gradient [40, 41]. The model was found to produce stiff profiles, power degradation, an anomalous system size scaling of confinement and rapid transport events, suggesting its general relevance to fusion transport studies. In the fluid limit, the model generates effective diffusive coefficients and pinch terms, which arise from the combination of finite-size particle steps and the critical mechanism, and may provide a partial explanation of the anomalous pinches observed in fusion experiments. Firm conclusions can, however, only be drawn on the basis of a more complete model (for at least two fields, n and T), which is currently under development.

3.2. *Radial electric fields and transport*

Radial plasma potential profiles have been obtained in the TJ-II by the HIBP diagnostic. These profiles show that the potential increases up to 1 kV near the magnetic axis in low-density plasmas ($n_e < 8 \times 10^{18}\,\mathrm{m^{-3}}$) (figure 10). In addition, the plasma potential shows a strong dependence on the plasma density. This finding is in reasonable agreement with neoclassical simulations for similar plasma conditions [42]. A recently developed Monte-Carlo code has been used to compute global ion fluxes in different TJ-II magnetic configurations [43]. These new simulations indicate that a non-local transport treatment might be important in complex devices like TJ-II. The secondary (Cs^{++}) beam ion current profiles, which directly reflect the plasma density, are hollow (figure 10). Such hollow profiles may be a manifestation of an outward particle flux induced by ECRH (i.e. the pump-out effect). Also, it has been experimentally observed that the modification of the profile shape is dependent on the position of low-order rational surfaces, while the degree of profile hollowness is qualitatively correlated with the magnitude of the convective flux of ripple-trapped suprathermal electrons [44]. An approach based on Langevin equations has been recently developed to estimate this ECRH induced flux [45].

An ion power balance analysis based on central ion temperatures, obtained with a neutral particle analyser, and electron temperature and density profiles indicate the existence of two different confinement regimes (which can

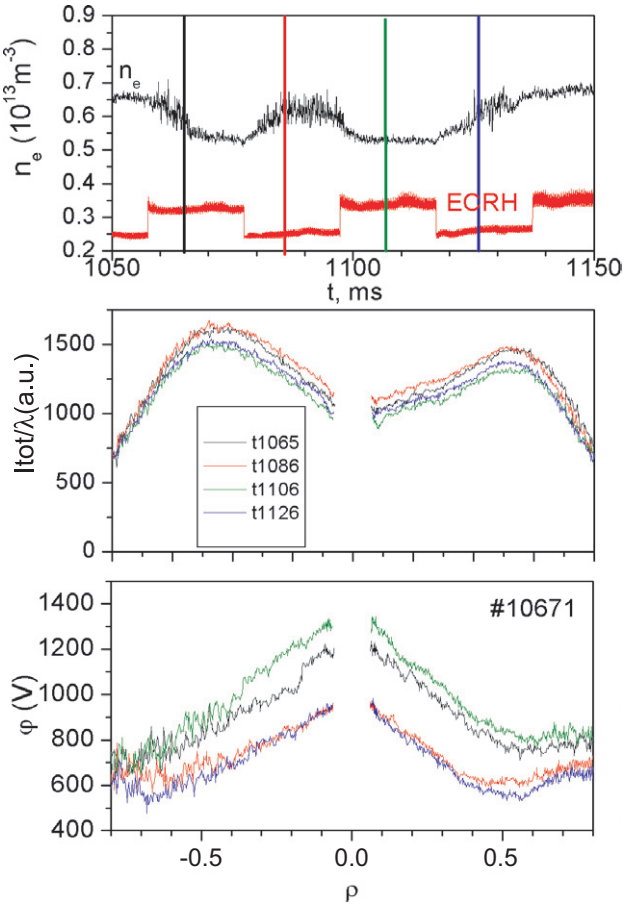

Figure 10. Time evolution of heating power and plasma density (top) and plasma potential and secondary Cs^{2+} ion profiles. The global plasma density decreases as ECRH power increases whereas the plasma potential becomes more positive. Density profiles (as measured by the HIBP system) become more hollow.

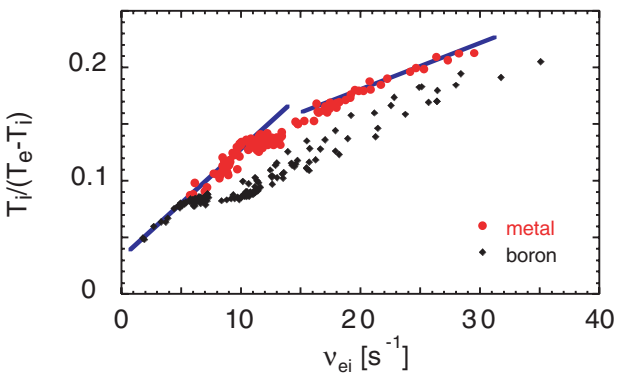

Figure 11. Influence of plasma collisionality on ion transport.

be defined by electron–ion collisionality) characterized by two ion energy confinement times (both in the range of several ms) (figure 11). The transition between these regimes, which depends on wall conditioning, is also compatible with changes in the estimated ambipolar electric field deduced from neoclassical calculations [42, 46].

The influence of low-order rational surfaces (e.g. $n = 4/m = 2, \iota(a)/2\pi \approx 2$) on the structure of parallel flows and plasma potential is under investigation. The presence of

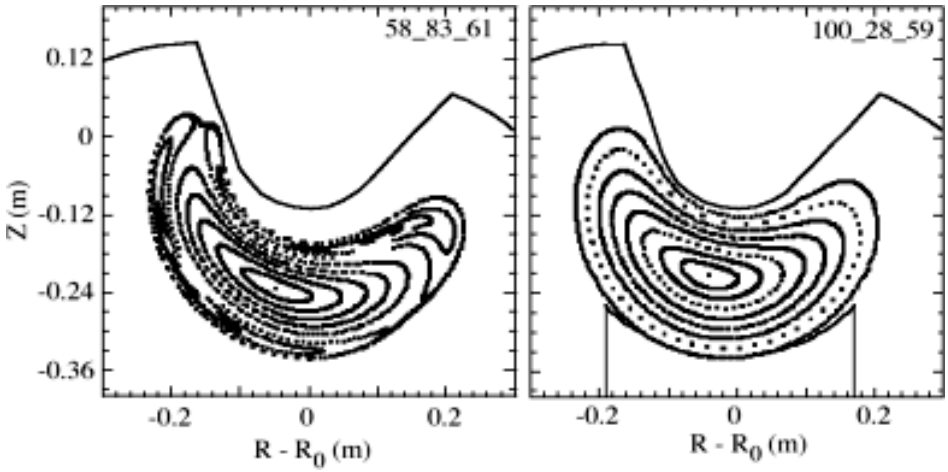

Figure 12. Two examples of the magnetic configurations used in the experiments: an example of a 'divertor-type' configuration (left): a 'standard' configuration (right).

natural resonant surfaces has been deduced from a flattening observed in plasma-edge ion saturation current profiles, i.e. the floating potential becomes more positive and shows a significant radial variation. Quasi-coherent modes (of about 70 kHz), associated with the existence of rational surfaces, have been observed in the TJ-II. Moreover, differences in parallel-flow profiles exist in configurations with and without low-order rationals: a minimum appears to the outside of the rational location whereas this minimum does not appear in configurations free of rationals [47]. A possible explanation for such a flow structure near rational surfaces is the coupling of flow generation and turbulence [48]. This mechanism is consistent with the magnitude of the observed shearing rates (which are close to the critical value for reducing fluctuations) in the vicinity of a magnetic island. More recently, it has been shown that, in the framework of neoclassical mechanisms, radial gradients can also be expected near rational surfaces in the radial electric fields [49].

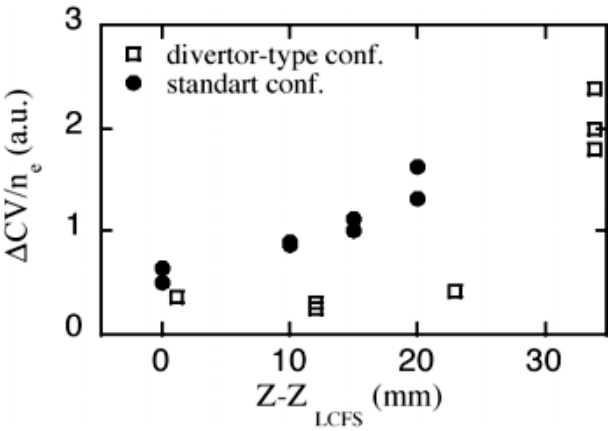

Figure 13. Evolution of the normalized CV contamination at different radial positions of the impurity puff, for both configurations: (●) for 'standard' and (□) for 'divertor-type' configurations.

4. Plasma–wall studies: divertor like configurations

Recent TJ-II experiments have focused on configurations with a low-order rational value in the rotational transform located in the proximity of the last closed flux surface ($n = 4/m = 2$), eventually leading to 'local island divertor' topologies. Hydrocarbon fuelling experiments in these configurations have been used to characterize the impurity screening properties related to the expected divertor effect (figure 12).

A different response to the same injected impurity was observed for edge-island configurations when compared to standard ones. Furthermore, the intrinsic contamination of the divertor-type configurations is systematically lower than that of conventional ones [50]. Thus, in the ethylene puffing experiments, a much lower increase of the normalized central carbon impurity (C V and C VI lines) takes place under 'divertor' configuration scenarios. The relative decrease of the hydrocarbon fuelling efficiency in divertor-type configurations is a strong function of the injection point location. This is shown in figure 13, where the normalized C V intensity is plotted versus the location of the poloidal limiter carrying the gas inlet. Note that all the positions shown correspond to the nominal confined, edge plasma region. A sudden enhancement of central carbon emission takes place at a critical radial location of the limiter. This position is well correlated with the nominal position of the actual separatrix in the divertor-type configuration (figure 12). In standard configurations, however, a gradual increase of the fuelling efficiency is observed. It is worth noting that even when the injection point of these experiments corresponds to the confined region, the contamination of the plasma is very low. This suggests the presence of a weakly confining region in the last 2–3 cm of the plasma, as inferred from the plasma edge profiles [7], and the prompt decomposition of the injected molecular species at the plasma edge of TJ-II.

5. NBI plasmas

The first experiments with NBI heated plasmas have been performed in the TJ-II stellarator. Flattened core electron

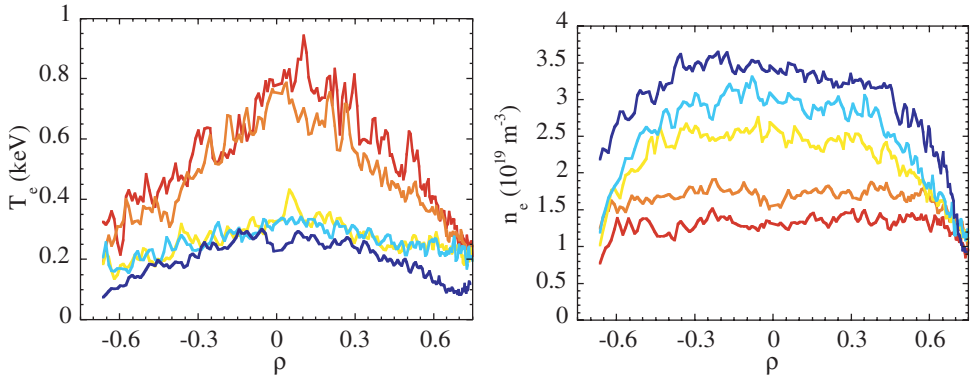

Figure 14. Density and electron temperature profiles during the transition from ECRH (black) to NBI (grey) plasmas.

temperatures in the range 200–300 eV and bell-shaped density profiles with $n_e \leqslant 5 \times 10^{19}\,\mathrm{m}^{-3}$ are achieved in NBI plasmas (200 kW) (figure 14). In comparison, TJ-II ECRH (200–400 kW) plasmas show flat or hollow density profiles with steep temperature profiles. Power balance estimates show that the NBI Thomson scattering profiles correspond to significant central power deposition.

The behaviour of the plasma ions and impurities has also been studied at the transition between ECH and NBI regimes. The ion temperature as measured by a neutral particle analyser shows a non-Maxwellian spectrum with a first slope that evolves from 90 eV under ECH to around 130 eV under NBI. Impurity temperature and rotation are monitored using passive emission spectroscopy. Toroidal rotation in both directions (co and counter) has been observed and it is seen to vary widely in magnitude (from a few to tens of $\mathrm{km\,s}^{-1}$) [51].

Computer simulations of the beam–plasma interaction with the Monte-Carlo code FAFNER combined with the transport code PROCTR allow us to calculate NBI absorption, fuelling and plasma electric field. The self-consistent ambipolar radial electric field resulting from PROCTR is always negative with NBI, while for ECRH discharges it is positive near the axis. Preliminary measurements of plasma potential with the heavy ion beam diagnostic confirm the evolution of the electric field from positive for ECH plasmas to near sign reversal for the NBI regime.

Combined ECRH and NBI experiments reveal that, once ECRH heating power is switched off, a confinement regime characterized by a strong reduction in $E \times B$ turbulence and a significant increase in the ratio between density and particle recycling (H_α) is achieved. Several modes below 300 kHz have been found in the frequency spectra of magnetic pick-up coils in the NBI regime, which can be interpreted as Alfvén modes. The SOL density decay length decreases to half its ECRH value and the tails in density profiles, currently observed in the SOL region in ECRH plasmas, disappear in the NBI phase. These results provide the first observation of a direct link between the statistical properties of turbulent transport and non-exponential (and even flat) density profiles in the SOL region.

The maximum density reached ($\approx 4 \times 10^{19}\,\mathrm{m}^{-3}$) falls within the stellarator density limit scaling law, suggesting that TJ-II NBI discharges terminate when their intrinsic density limit is reached. Experimental results suggest the importance of both radiative and edge transport mechanisms in the physics of the density limit of TJ-II.

Different combinations of gas puffing, ECH heating and wall conditioning strategies have been investigated with the aim of optimizing the power coupling and density control for NBI plasmas. Density control in NBI discharges with a plasma target created by on-axis ECH has proved difficult. Repeated wall cleaning seems to help only to the extent of smoothing the density rise, although there appears no sign of stabilizing its value. In contrast, target plasmas created by off-axis ECH, maintained during the NBI phase, are promising. In this way NBI plasma discharges with density control (up to 130 ms) have been obtained.

6. Conclusions

Significant improvements in characterizing the confinement and stability properties of TJ-II stellarator plasmas have been achieved recently.

Global confinement studies have shown a positive dependence of energy confinement on rotational transform and density, together with different parametric dependences for metallic and boronized wall conditions. Spontaneous and biasing-induced improved confinement transitions have been observed. The phenomenology of TJ-II improved confinement regimes (a device designed for high beta operation but not optimized for neoclassical transport) looks similar to the H-mode regimes previously reported in stellarators.

Magnetic configuration scan experiments have highlighted the interplay between magnetic topology (rationals, magnetic shear), transport and electric fields. Dc radial electric fields are comparable with those expected from neoclassical calculations. However, additional mechanisms based on neoclassical–turbulent E_r bifurcations and kinetic effects are needed to explain the impact of magnetic topology on transport. Hydrocarbon fuelling experiments in configurations with a low-order rational value in the rotational transform located in the proximity of the last closed flux surface ($n = 4/m = 2$) have shown the impurity screening properties related to the expected divertor effect.

The first experiments in NBI plasmas have been performed in the TJ-II stellarator. The evolution of transport, density and turbulence at the transition from ECRH to NBI plasmas points in the direction of an improved particle confinement regime.

References

[1] Ascasibar E. *et al* 2002 *Plasma Phys. Control. Fusion* **44** B307
[2] Castellano J. *et al* 2002 *Phys. Plasmas* **9** 713
[3] Cappa A. *et al* 2004 *Nucl. Fusion* **44** 406
[4] Liniers M. *et al* 1998 *Fusion Technol.* **1** 307
[5] Ascasibar E. *et al* 2005 *Nucl. Fusion* **45** 276
[6] Stroth U. *et al* 1996 *Nucl. Fusion* **30** 1063
[7] Tabarés F.L. 2001 *Plasma Phys. Control. Fusion* **43** 1023
[8] Tabarés F. *et al* 2003 *J. Nucl. Mater.* **313** 839
[9] García-Cortés I. *et al* 2002 *Plasma Phys. Control. Fusion* **44** 1639
[10] Hidalgo C. *et al* 2004 *Phys. Rev.* E **70** 067402
[11] Pedrosa M.A. *et al* 2005 *Plasma Phys. Control. Fusion* **47** at press
[12] Romero J. *et al* 2003 *Nucl. Fusion* **43** 386
[13] López-Bruna D. *et al* 2004 *Nucl. Fusion* **44** 645
[14] Wolf R.C. 2003 *Plasma Phys. Control. Fusion* **45** R1
[15] Fujisawa F. *et al* 1999 *Phys. Rev. Lett.* **29** 2669
[16] Stroth U. *et al* 2001 *Phys. Rev. Lett.* **86** 5910
[17] Ida K. *et al* 2003 *Phys. Rev. Lett.* **91** 085003
[18] Fujisawa A. 2003 *Plasma Phys. Control. Fusion* **45** R1
[19] Lopes Cardozo N. *et al* 1997 *Plasma Phys. Control. Fusion* **39** B303
[20] Joffrin E. *et al* 2003 *Nucl. Fusion* **43** 1167
[21] Hidalgo C. *et al* 2000 *Plasma Phys. Control. Fusion* **42** A153
[22] Ida K. *et al* 2000 *Phys. Rev. Lett.* **88** 015002
[23] Romanelli F. and Zonca F. 1993 *Phys. Fluids* B **5** 4081
[24] Brakel R. *et al* 2002 *Nucl. Fusion* **42** 903
[25] Garbet X. *et al* 2003 *Nucl. Fusion* **43** 975
[26] Candy J. *et al* 2004 *Phys. Plasmas* **11** 1879
[27] Estrada T. *et al* 2004 *Plasma Phys. Control. Fusion* **46** 277
[28] Castejón F. *et al* 2004 *Nucl. Fusion* **42** 593
[29] Estrada T. *et al* 2002 *Plasma Phys. Control. Fusion* **44** 1615
[30] Hidalgo C. *et al* 2004 *Plasma Phys. Control. Fusion* **45** 287
[31] Melnikov A. *et al* 2004 *Fusion Sci. Technol.* **46** 299
[32] McCarthy K.J. *et al* 2004 *Fusion Technol.* **46** 129
[33] Erkmann V. *et al* 1993 *Phys. Rev. Lett.* **70** 2086
[34] Okamura S. *et al* 2004 *Plasma Phys. Control. Fusion* **46** A113
[35] Zurro B. *et al* 2003 Transport analysis of impurity injected by laser ablation in the TJ-II stellarator *Proc. 30th EPS on Controlled Fusion and Plasma Physics (St Petersburg)* vol 27A p-2.79
[36] Zurro B. *et al* 2004 *Rev. Sci. Instrum.* **75** 4231
[37] Burhenn R. *et al* 1999 *Rev. Sci. Instrum.* **70** 603
[38] Eguilior S. *et al* 2003 Perturbative particle transport experiments on TJ-II stellarator *Proc. 14th Int. Stellarator Workshop* (*Greifswald*) (in CD rom)
[39] Van Milligen B. *et al* 2002 *Nucl. Fusion* **42** 787
[40] Van Milligen B. *et al* 2004 *Plasma Phys.* **11** 3787
[41] Van Milligen B. *et al* 2004 Phys. Plasmas **11** 2272
[42] Tribaldos V. 2001 *Phys. Plasmas* **8** 1229
[43] Tribaldos V. *et al* 2005 *Plasma Phys. Control. Fusion* **47** 545
[44] Ochando M.A. *et al* 2003 *Plasma Phys. Control. Fusion* **45** 221
[45] Castejón F. and Eguilior S. 2003 *Plasma Phys. Control. Fusion* **45** 159
[46] Balbín R. *et al* 2003 Ion confinement studies on the TJ-II stellarator *Proc. 14th Int. Stellarator Workshop* (*Greifswald*)
[47] Pedrosa M.A. *et al* 2004 *Plasma Phys. Control. Fusion* **46** 221
[48] Hidalgo C. *et al* 2002 *New J. Phys.* **5** 51
[49] Shaing K.C. *et al* 2003 *Nucl. Fusion* **43** 258
[50] García-Cortés I. *et al* 2005 *J. Nucl. Mater.* **337** 441
[51] Rapisarda D. *et al* 2004 Toroidal rotation of protons and impurities in the TJ-II stellarator: ECRH versus umbalanced NBI *Proc. 31th EPS Conf. on Plasma Physics (London)* p4-173